Integration of Improved Flux Linkage Observer and *I–f* Starting Method for Wide-Speed-Range Sensorless SPMSM Drives

Qipeng Tang, Duxin Chen, *Member, IEEE*, and Xiangning He, *Fellow, IEEE*

***Abstract*—This article aims to improve the sensorless control performance of surface-mounted permanent magnet synchronous machine drives in the whole speed range. Based on the thought of speed partition optimization and smooth transition, a hybrid sensorless control strategy integrating with an improved flux linkage observer and the current–frequency (*I–f*) starting method is proposed. At zero–low speed, the *I–f* control method is utilized for the stable startup and strong antijamming capability. At medium–high speed, an improved flux linkage observer based on the sliding-mode compensator is designed for the closed-loop sensorless operation. Taking advantage of the sliding-mode compensator, not only the position estimation errors caused by the adopted filter can be compensated effectively without any speed iteration to improve the system stability, but also the suitable cutoff frequency of the filter can be selected for the fast system dynamic response. Meanwhile, the influence of machine parameter variations on the rotor-position estimation accuracy is discussed. Furthermore, in order to achieve the smooth operation between two different control schemes, an adaptive transition algorithm is described in detail. Experimental results indicate that the proposed hybrid sensorless control strategy can show an excellent performance for both steady-state and dynamic operations during full-speed range.**

***Index Terms*—Adaptive transition algorithm, hybrid sensorless control strategy, sliding-mode compensator, surface-mounted permanent magnet synchronous machine (SPMSM).**

NOMENCLATURE

$V_{\alpha\beta}$, V_{dq}, $V_{\delta\gamma}$	Stator voltage vector.
$i_{\alpha\beta}$, i_{dq}, $i_{\delta\gamma}$	Stator current vector.
i_d, i_q	*d*-axis and *q*-axis currents.
i_d*, i_q*	*d*-axis and *q*-axis expected currents.
R_s, R_{s0}, ΔR_s	Actual value, measured value, and variations of stator resistance.
$\psi_{\rm pm}$, $\psi_{\rm pm0}$, $\Delta\psi_{\rm pm}$	Actual value, measured value, and variations of flux linkage generated by permanent magnet.
θ_r	Actual rotor-position
L_s, L_{s0}, ΔL_s	Actual value, measured value, and variations of stator inductance.
ω_r, ω_r*	Actual value and expected value of rotor speed.
n_p	Number of pole pairs of rotor.
T_e	Magnetic torque.
J	Motor inertia.
$\theta_{r\rm Est}$	Estimated position
θ_{I-f}	Orientation angle during the *I–f* start-up stage.
φ	Space vector angle of transient current relative to the *d*-axis.
I_s	Magnitude of transient stator current.
K	Gain of sliding-mode compensator.
$K_{\omega1}$, $K_{\omega2}$	Two switching coefficients.
j	Imaginary unit.
d/dt	Derivative operator.
$\alpha\beta$, dq, $\delta\gamma$	Subscript: stationary reference frame ($\alpha\beta$), synchronous rotating reference frame (dq), defined frame with the synchronous rotational frequency ($\delta\gamma$).

Manuscript received August 24, 2019; revised November 11, 2019; accepted December 25, 2019. Date of publication December 30, 2019; date of current version April 22, 2020. This work was supported in part by the National Key Research and Development Program of China under Grant 2017YFE0112400, in part by the National Natural Science Foundations of China under Grants 51690182 and 51677166, and in part by the Youth Program of National Natural Science Foundation of China under Grants 51907174 and 61903079. Recommended for publication by Associate Editor D. G. Xu. *(Corresponding author: Duxin Chen.)*

Q. Tang and X. He are with the College of Electrical Engineering, Zhejiang University, Hangzhou 310027, China (e-mail: d201377541@163.com; hxn@zju.edu.cn).

D. Chen is with the Jiangsu Key Laboratory of Networked Collective Intelligence, School of Mathematics, School of Automation, Southeast University, Nanjing 210096, China (e-mail: chendx@seu.edu.cn).

Color versions of one or more of the figures in this article are available online at http://ieeexplore.ieee.org.

Digital Object Identifier 10.1109/TPEL.2019.2963208

I. INTRODUCTION

IN RECENT decades, surface-mounted permanent magnet synchronous machines (SPMSMs) have been extensively applied in various drive fields ranging from servo drives, robotics, electric vehicles to aerospace engineering owing to their superior characteristics, such as high efficiency, high power density, high torque-to-volume ratio, wide speed range, and reliable operations. As the essential information in the high-performance field-oriented control (FOC) system, the accurate rotor-position is often obtained from the shaft-mounted mechanical encoders, which, in turn, may result in the reduction of robustness, additional volume and limited applications in high-frequency vibration and humidity, and high-temperature environment. Therefore, the position sensorless control of SPMSMs have attracted more and more attentions [1]–[28].

According to different control structures, sensorless control solutions can be divided into two categories: open-loop sensorless control solutions and closed-loop sensorless control solutions. As the typical open-loop sensorless control solution, the *V–f* control method is widely used in the practical applications due to its low-cost implementation feasibility and insensitivity to application environment [1], [2]. However, the *V–f* control solution easily loses synchronization and even damages electronics devices under heavy load starting or abrupt load change conditions if the ratio of voltage and frequency is selected improperly. Thus, stabilizing loops are required to improve the stability of the conventional *V–f* control solutions [2]. In comparison with the *V–f* control method, the *I–f* control solution has the current closed-loop regulator to generate the desired voltage [3]–[5], which can fulfill stable startup of the machine through its intrinsic self-stabilization between torque and power angle, enable to prevent current overshoot effectively by current regulation and possess the ability of antidisturbance to a degree. However, because the amplitude of the stator current cannot be regulated automatically, additional reactive power loss will be generated, especially under the light applied load. Hence, the open-loop *I–f* control strategy is mainly utilized as an auxiliary measure for the startup.

In closed-loop sensorless control solutions, the knowledge of the rotor-position is crucial. According to the different principles for the acquisition of the rotor-position information, closed-loop sensorless control solutions can be further categorized into two types: high-frequency carrier signal injection methods [6]–[10], and model-based methods [11]–[28]. The high-frequency carrier signal injection methods are based on the magnetic saliency detection by injecting a high-frequency signal to interact with rotor-position-dependent saliencies. Although these methods are independent of the back electromotive force (EMF) and machine parameters and may show good performance at zero–low speed, they face some problems of extra losses, torque ripple, high-frequency noise, and limited control performance caused by the additional filter as the machine speed increases. Model-based methods are silent algorithms that do not utilize signal injection, which mainly include the back-EMF estimation methods [11]–[18] and the flux linkage estimation methods [19]–[28]. These methods can work reasonably well in middle- and high-speed regions. Nevertheless, as the speed decreases, the rotor-position may be obtained inaccurately because the reduction and eventual disappearance of the back-EMF is too small to give reliable information about the rotor-position at low or zero speeds. Therefore, in order to achieve sensorless control of the SPMSM in the whole speed range, hybrid position estimation strategies combining the abovementioned two categories are usually adopted [18]–[20]. And because most drive devices usually operate at medium–high speed for long to achieve higher efficiency, the control performance of model-based methods is mainly considered in this article. In contrast to the back-EMF estimation method, the flux linkage estimation method is expected to achieve the wider speed range sensorless operations because the rotor flux linkage does not vanish and remains almost constant at any speed, which has attracted more and more scholars' attentions. However, it also faces some practical issues of dc drifting and harmonics because a pure integrator is normally required to calculate the flux linkage term. Therefore, a number of methods have been presented to overcome these issues [21]–[28]. An accurate flux linkage acquisition method with online correction approach of the drift and residual errors from the drive system is described in [21]. An excellent flux linkage estimation performance down to a 1.3-Hz stator frequency has been obtained by advocating a pure integration based on the simple resonant-type observer design. In [22], an integration algorithm of a fifth-order filter, a high-pass filter, and a logical calculation part is investigated for stator flux linkage estimation, which can achieve same amplitude and phase-frequency characteristics as those of the pure integrator at any synchronous angular frequency. In [24], a new flux linkage estimation method based on the dual second-order generalized integrator frequency-locked loop is presented, which can not only effectively attenuate dc drifting and the high-order harmonics, but also improve the dynamic response. In [26], a nonlinear observer based on the linear regression model is constructed for sensorless control of the interior permanent magnet synchronous machine (IPMSM) and a pseudo-high-pass filter is applied to eliminate the effects of dc bias. And the Gopinath model flux linkage observer that combines the current and voltage model is utilized to eliminate dc saturation and dc drift problems in [27]. Among these flux linkage-based estimation methods, either the low-pass filter (LPF) with the corresponding angle compensation solution or the closed-loop flux linkage observer is utilized to eliminate dc saturation and dc drift problems, which may not only increase the speed iterative operation but also bring a careful consideration of the system stability.

This article aims to improve the sensorless control performance of the SPMSM in the whole speed range. Based on the thought of speed partition optimization and smooth transition, a hybrid sensorless control strategy integrating with an improved flux linkage observer and the *I–f* starting method is proposed. At zero and low speed, the stable startup and the ability of antidisturbance to a degree can be obtained by utilizing its self-stabilization between torque and power angle of the *I–f* control method. At medium and high speed, an improved flux linkage observer based on the sliding-mode compensator is designed for the closed-loop sensorless operation. Taking advantage of the sliding-mode compensator, these position errors caused by the adopted filter for the elimination of dc offset and high-order harmonics can be compensated accurately without any speed iteration no matter how large these position errors, which not only can effectively improve the system stability, but can also achieve the fast system dynamic response by selecting the suitable cutoff frequency of the filter. Meanwhile, the influence of machine parameter variations on the rotor-position estimation accuracy is discussed. Furthermore, in order to achieve a smooth operation between two different control schemes, an adaptive transition algorithm is described in detail. Experimental results indicate that the proposed hybrid sensorless control strategy can show an excellent performance for both steady-state and dynamic operations during full-speed range.

This article is arranged as follows. In Section II, the conventional flux linkage estimation method is described. An improved flux linkage observer based on the sliding-mode compensator is designed in Section III. Meanwhile, the influence of machine parameter variations is analyzed in detail. In order to achieve the

full-speed-range sensorless control of the PMSM, an open-loop *I–f* starting with an adaptive transition algorithm is presented in Section IV. In Section V, the experimental results verify the effectiveness and feasibility of the proposed hybrid sensorless control system. Finally, Section VI concludes this article.

II. Conventional Flux Linkage Estimation Method

Regardless of the cross coupling and multisaliency of the machine, the basic mathematical model of the SPMSM can be described as (1) using complex vector in the α–β stationary reference frame

$$V_{\alpha\beta} = R_s i_{\alpha\beta} + L_s \frac{d}{dt} i_{\alpha\beta} + j\omega_r \psi_{\rm pm} e^{j\theta_r}. \tag{1}$$

When the machine runs at medium and high speed, the rotor flux linkage $\psi_{\alpha\beta r}$ can be used to obtain the rotor-position by calculating the flux linkage induced by the rotor magnets into the stator windings, which can be expressed as (2) by rearranging (1)

$$\psi_{\alpha\beta r} = \psi_{\rm pm} e^{j\theta_r} = \int (V_{\alpha\beta} - R_s i_{\alpha\beta})\, dt - L_s i_{\alpha\beta}. \tag{2}$$

However, in the practical applications, in order to eliminate these issues of dc offset and harmonics due to initial rotor flux linkage, detection errors, etc., an LPF is usually adopted instead of the pure integrator in (2), as expressed in (3a). And then, the rotor-position can be calculated as (3b)

$$\psi_{\alpha\beta r1} = {\rm LPF}\,(V_{\alpha\beta} - R_s i_{\alpha\beta}) - L_s i_{\alpha\beta} \tag{3a}$$

$$\theta_{rEst} = {\rm Arg}\,(\psi_{\alpha\beta r1}) \tag{3b}$$

where Arg(x) represents the phase angle of the vector $\boldsymbol{x}$. As observed from (3), the calculation of the rotor-position is based on the interior electromagnetic relationship of the machine by using the real-time measurements of the stator voltages and currents, which guarantees the fast dynamic response speed. However, the adopted LPF not only brings inevitable phase and amplitude deviations related to its own cutoff frequency and the angular frequency of the input signal, but also reduces the system bandwidth. The lower cutoff frequency brings the smaller position errors, but leads to the slower dynamic response. Although some compensation solutions can be used, the effect of compensation is badly affected by the estimated value of real-time angular velocity. Therefore, it is hard to achieve the excellent sensorless control performance of the SPMSM by only adjusting the cutoff frequency of the adopted LPF in the conventional flux linkage estimation method.

III. Proposed Improved Flux Linkage Observer Based on Sliding-Mode Compensator

The contradiction of position estimation accuracy and dynamic response speed is the main reason why the excellent sensorless control performance of the SPMSM cannot be achieved in the conventional flux linkage estimation method. If the accurate and real-time compensation for the position estimation errors can be achieved under any LPF's cutoff frequency conditions, the efficient sensorless control of the SPMSM with excellent dynamic response speed can be easily implemented.

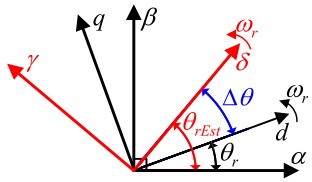

Fig. 1. Spatial relations of θ_r and $\theta_{r\rm Est}$.

Therefore, in order to achieve this purpose, an improved flux linkage observer based on the sliding-mode compensator is designed in this section.

A. Sliding-Mode Compensator

According to the abovementioned analysis, their spatial relationships of θ_r and $\theta_{r\rm Est}$ can be roughly described in Fig. 1, where $\Delta\theta = \theta_r - \theta_{r\rm Est}$ presents the position estimation errors, and the δ–γ reference frame is defined along the $\theta_{r\rm Est}$ direction. Considering that the convergence process of the LPF can be approximately ignored when its cutoff frequency is selected high enough, the rotational frequency of the defined δ–γ reference frame can be approximate to the synchronous frequency ω_r. As observed from Fig. 1, the rotor-position θ_r can be divided into two components: the estimated position $\theta_{r\rm Est}$, and position errors $\Delta\theta$. Since the estimated position $\theta_{r\rm Est}$ can be calculated by (3) with the suitable cutoff frequency of the LPF for rapid convergence speed, the keystone and difficulty are how to get the accurate position errors $\Delta\theta$.

In order to get the accurate position errors $\Delta\theta$, the position errors model can be deduced as (4) by transforming (1) into the defined δ–γ reference frame

$$V_{\delta\gamma} = R_s i_{\delta\gamma} + L_s \frac{d}{dt} i_{\delta\gamma} + j\omega_r \left(L_s i_{\delta\gamma} + \psi_{\rm pm} e^{j\Delta\theta}\right). \tag{4}$$

It can be seen from (4) that the last term $j\omega_r(L_s i_{\delta\gamma} + \psi_{\rm pm} e^{j\Delta\theta})$ on the right can be equivalently regarded as the back-EMF component, which contains the rotor-position estimation errors information $\Delta\theta$. The sliding-mode observer (SMO) is commonly used to observe the back-EMF signals due to its high robustness, insensitivity to motor parameter variations, and load disturbance. According to (4), the SMO can be expressed as

$$\frac{d\hat{i}_{\delta\gamma}}{dt} = \frac{1}{L_s} V_{\delta\gamma} - \frac{R_s}{L_s} \hat{i}_{\delta\gamma} - j\frac{K}{L_s} {\rm sgn}\left(\hat{i}_{\delta\gamma} - i_{\delta\gamma}\right) \tag{5}$$

where $\hat{i}_{\delta\gamma}$ are the observed current components in the δ–γ reference frame, and sgn(x) is the sign switching function. Designing the sliding-mode surface as $(\hat{i}_{\delta\gamma} - i_{\delta\gamma})$, and subtracting (4) from (5) yields

$$\frac{d}{dt}\left(\hat{i}_{\delta\gamma} - i_{\delta\gamma}\right) = -\frac{R_s}{L_s}\left(\hat{i}_{\delta\gamma} - i_{\delta\gamma}\right) - j\frac{K}{L_s}{\rm sgn}\left(\hat{i}_{\delta\gamma} - i_{\delta\gamma}\right) + j\frac{\omega_r}{L_s}\left(L_s i_{\delta\gamma} + \psi_{\rm pm} e^{j\Delta\theta}\right). \tag{6}$$

When the system reaches the sliding surface where the observed current deviations $(\hat{i}_{\delta\gamma} - i_{\delta\gamma})$ and their differentiations are equal to zero, the equivalent back-EMF term $j\omega_r(L_s i_{\delta\gamma} + \psi_{\rm pm} e^{j\Delta\theta})$ can be easily obtained by arranging (6). However, considering that the bang–bang control with a sign switching

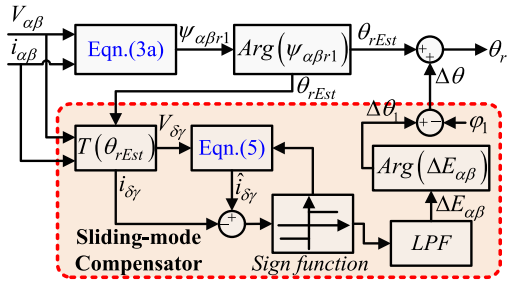

Fig. 2. Signal processing of the proposed flux linkage observer based on the sliding-mode compensator.

function is a discontinuous control that is susceptible to chattering, an LPF is usually adopted to filter the chattering, and the component $\Delta E_{\alpha\beta}$ that contains the rotor-position estimation errors information $\Delta\theta$ can be estimated as (7a). And then, the rotor-position estimation errors $\Delta\theta$ can be calculated as (7b)

$$\begin{aligned}\Delta E_{\alpha\beta} &= \mathrm{LPF}\left\{K\ \mathrm{sgn}\left(\hat{i}_{\delta\gamma}-i_{\delta\gamma}\right)\right\}\\ &= \omega_r\left(L_s i_{\delta\gamma}+\psi_{\mathrm{pm}}e^{j\Delta\theta}\right)=\omega_r\psi_{\mathrm{pm1}}e^{j(\Delta\theta+\varphi_1)} \quad (7a)\\ \Delta\theta_1 &= \mathrm{Arg}\left(\Delta E_{\alpha\beta}\right),\quad \Delta\theta=\Delta\theta_1-\varphi_1 \quad (7b)\end{aligned}$$

with

$$\begin{aligned}\psi_{\mathrm{pm1}} &= \sqrt{L_s^2I_s^2+\psi_{\mathrm{pm}}^2+2L_sI_s\psi_{\mathrm{pm}}\cos\varphi}\\ \varphi_1 &= \tan^{-1}\left(\frac{L_sI_s\sin\varphi}{L_sI_s\cos\varphi+\psi_{\mathrm{pm}}}\right). \quad (8)\end{aligned}$$

To further obtain the accurate rotor-position estimation errors $\Delta\theta$, φ_1 in (7b) should be determined. According to the calculation expression of φ_1 in (8), φ_1 is always changing with the stator current space vector angle φ. Thus, when the rotor-position θ_r and $i_d=0$ are used to implement the FOC of the SPMSM, the stator current space vector angle φ will be equal to $\pi/2$. And then, substituting $\varphi=\pi/2$ into (8) yields

$$\varphi_1=\tan^{-1}\left(\frac{L_sI_s}{\psi_{\mathrm{pm}}}\right). \quad (9)$$

Combining (7b) and (9), the accurate position estimation errors $\Delta\theta$ can be obtained when some parameter identification methods are referred [28]–[30] to get the accurate L_s and ψ_{pm}. And then, the summation of $\theta_{r\mathrm{Est}}$ and $\Delta\theta$ is the accurate rotor-position θ_r. The total signal processing of the proposed improved flux linkage observer based on the sliding-mode compensator can be depicted in Fig. 2. In which, $T(\theta_{r\mathrm{Est}})$ is the coordinate transformation matrix, which is used to transform the variables from the α–β stationary reference frame into the defined δ–γ reference frame. It is worthy noting that the adopted LPF has no influence on the estimation of $\Delta E_{\alpha\beta}$ in (7a) because $\Delta E_{\alpha\beta}$ is approximately constant and the fact that the LPF has no effects on the direct current input signals is always valid. As observed in Fig. 2, no matter how large these angle deviations between $\theta_{r\mathrm{Est}}$ and the actual rotor-position θ_r, they can be always compensated accurately by using the sliding-mode compensator without any speed iteration, which can effectively improve the system stability. Furthermore, because these angle deviations between $\theta_{r\mathrm{Est}}$ and θ_r have no influence on the estimation accuracy of the rotor-position, the suitable cutoff frequency of the LPF in (3a) can be selected for the fast system dynamic response. Therefore, the efficient sensorless control of the SPMSM with excellent dynamic response speed can be achieved by using the proposed improved flux linkage observer based on the sliding-mode compensator.

B. Effects of Machine Parameter Variations

In the abovementioned analysis, machine parameter variations are neglected. However, in the practical implementation, the stator resistance R_s, the stator inductance L_s, and flux linkage of the rotor magnet ψ_{pm} are inaccurate and varying according to the operating conditions, such as rotor temperature and saturation of the machine. Especially at high speed with heavy applied load, some variations of the stator inductance may bring larger errors in the rotor-position estimation. Therefore, the robustness of the proposed improved flux linkage observer against machine parameter variations is discussed in this section.

According to the signal processing in Fig. 2, with the proposed improved flux linkage observer, the influence of machine parameter variations on the estimated rotor-position $\theta_{r\mathrm{Est}}$ can be seen as a part of the LPF, and the estimation accuracy of the rotor-position is only determined by the position estimation errors $\Delta\theta$. Thus, considering machine parameter variations, the stator resistance R_s, the stator inductance L_s, and the rotor magnet flux linkage ψ_{pm} can be described as (10a), and (7a) can be written as (10b)

$$\begin{aligned}R_s &= R_{s0}+\Delta R_s, L_s=L_{s0}+\Delta L_s,\\ \psi_{\mathrm{pm}} &= \psi_{\mathrm{pm0}}+\Delta\psi_{\mathrm{pm}} \quad (10a)\\ \Delta E_{\alpha\beta\_v} &= \mathrm{LPF}\left\{K\cdot\mathrm{sgn}\left(\hat{i}_{\delta\gamma}-i_{\delta\gamma}\right)\right\}\\ &= \omega_r\left(L_si_{\delta\gamma}+\psi_{\mathrm{pm}}e^{j\Delta\theta}\right)-j\Delta L_s\frac{di_{\delta\gamma}}{dt}-j\Delta R_si_{\delta\gamma}. \quad (10b)\end{aligned}$$

According to the abovementioned analysis, the stator current in the δ–γ reference frame $i_{\delta\gamma}$ is approximately constant, and its differentiation is approximate to zero because their rotational frequencies of θ_r and $\theta_{r\mathrm{Est}}$ are approximately equal. Afterward, substituting $di_{\delta\gamma}/dt=0$ and $i_{\delta\gamma}=I_se^{j(\Delta\theta+\varphi)}$ into (10b) yields

$$\Delta E_{\alpha\beta\_v}=\mathrm{LPF}\left\{K\ \mathrm{sgn}\left(\hat{i}_{\delta\gamma}-i_{\delta\gamma}\right)\right\}=\omega_r\psi_{\mathrm{pm2}}e^{j(\Delta\theta+\varphi_{1\_v})} \quad (11a)$$

$$\Delta\theta_{1\_v}=\mathrm{Arg}\left(\Delta E_{\alpha\beta\_v}\right)=\Delta\theta+\varphi_{1\_v} \quad (11b)$$

with

$$\varphi_{1\_v}=\tan^{-1}\left(\frac{\omega_rL_sI_s\sin\varphi-\Delta R_sI_s\cos\varphi}{\omega_rL_sI_s\cos\varphi+\omega_r\psi_{\mathrm{pm}}+\Delta R_sI_s\sin\varphi}\right).$$

It should be noted that the concrete expression of ψ_{pm2} is not given because it has no effects on the rotor-position estimation. And, according to the description given in Fig. 2, the estimated rotor-position is equal to $(\Delta\theta_{1\_v}+\theta_{r\mathrm{Est}}-\varphi_1)$. And then, when $(\Delta\theta_{1\_v}+\theta_{r\mathrm{Est}}-\varphi_1)$ and $i_d=0$ are used to implement the FOC of the SPMSM, the stator current space vector angle φ

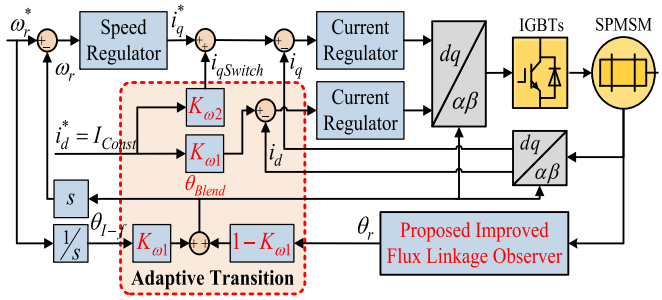

Fig. 3. Overall system block diagram of the proposed hybrid sensorless control strategy integrating with the improved flux linkage observer and the *I–f* starting method.

is equal to $(\Delta\theta_{1\_v} - \Delta\theta - \varphi_1 + \pi/2)$. Afterward, substituting $\varphi = (\Delta\theta_{1\_v} - \Delta\theta - \varphi_1 + \pi/2)$ into (11b) yields

$$\varphi_{1\_v} = \sin^{-1}\left(\frac{\omega_r L_s I_s \psi_{\mathrm{pm0}} - \Delta R_s L_{s0} I_s^2}{\omega_r \psi_{\mathrm{pm}} \sqrt{\psi_{\mathrm{pm0}}^2 + L_{s0}^2 I_s^2}}\right) \approx \sin^{-1}\left(\frac{L_s I_s \psi_{\mathrm{pm0}}}{\psi_{\mathrm{pm}} \sqrt{\psi_{\mathrm{pm0}}^2 + L_{s0}^2 I_s^2}}\right). \quad (12)$$

As observed from (12) and (9), φ_1 and φ_{1_v} are not equal when machine parameter variations are considered, which will lead to some rotor-position estimation errors $(\varphi_{1\_v} - \varphi_1)$. And, because the proposed improved flux linkage observer is usually suitable in the medium- and high-speed range, the effects of the stator resistance variations ΔR_s are little and can be neglected. It is evident from (12) that the accurate acquisition of L_s and ψ_{pm} helps to improve the rotor-position estimation accuracy. Therefore, several machine parameter identification methods should be adopted to identify L_s and ψ_{pm} online and accurately [28]–[30].

IV. Adaptive Transition Algorithm

It is noteworthy that the proposed improved flux linkage observer is only applicable in medium- and high-speed range. It fails in the low-speed region and usually suffers from starting problem because the reliable rotor-position information is hard to extract at low speed, including zero speed. Therefore, in order to achieve the wide-speed-range sensorless control of the PMSM, an open-loop *I–f* starting strategy with an adaptive transition to the closed-loop sensorless control based on the proposed improved flux linkage observer is developed in this section.

The *I–f* control is an open-loop method with a current regulator to generate the desired voltage, which is widely used for the machine start-up due to its stable startup and ability of antidisturbance to a degree. The overall system block diagram of the proposed hybrid sensorless control strategy is depicted in Fig. 3. During the *I–f* start-up stage, the applied reference speed ω_r^* is ramped by using a first-order delay filter, whereas the reference current is added on the *d*-axis and its amplitude is maintained constant, namely $i_d^* = K_{\omega 1} I_{Const}$. From this frequency, an imposed position θ_{I-f} is obtained. The orientation angle θ_{Blend} for the FOC of the SPMSM is obtained by blending

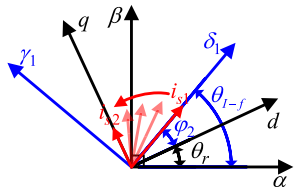

Fig. 4. Transition process from the *I–f* starting to the proposed improved-flux-linkage-observer-based closed-loop sensorless control strategy.

the imposed position θ_{I-f} and the rotor-position θ_r with the switching coefficient $K_{\omega 1}$. And, the prescribed phase current is commutated by using this feedforward signal. By setting the switching coefficient $K_{\omega 1}$ as 1, the feedforward speed signal ω_r is always equal to the reference speed $\omega_r^*$and the orientation angle θ_{Blend} is equal to θ_{I-f}, which keeps the speed regulator with zero input error to avoid error accumulation in the integral component. The initial value of another switching coefficient $K_{\omega 2}$ remains at zero. It should be noted that the amplitude of current I_{Const} is usually chose over the rated current of the machine to possess the sufficiently strong self-stabilization and ability with load. However, because I_{Const} cannot be regulated automatically, additional reactive power loss will be generated, especially under the light applied load. Thus, the *I–f* control open-loop strategy is only suitable for the startup.

As the speed increases, a reasonable switching algorithm from the *I–f* control to the proposed improved flux linkage observer should be conceived to achieve higher efficiency and control accuracy. In order to ensure a smooth transition without a large torque ripple and speed fluctuation, the switching algorithm should meet three requirements.

1) The orientation angle θ_{Blend} should be adjusted to θ_r from θ_{I-f}.
2) The *d*-axis current should decrease to zero from I_{Const}.
3) The large torque ripple and speed fluctuation should be avoided during the whole transition process.

For requirements 1 and 2, the switching coefficient $K_{\omega 1}$ gradually decreases to 0 from 1. For requirement 3, the electromagnetic torque should be controlled unchanged during the whole transition process under the assumption that the duration of the transition is very short and the reference speed and the applied load are unchanged. Fig. 4 shows the whole transition process. In which, $\delta_1 - \gamma_1$ is the controlled reference frame during the *I–f* start-up stage, which is always rotating with the reference speed ω_r^*. And $\varphi_2 = (\theta_{\mathrm{Blend}} - \theta_r)$, is the orientation angle errors relative to the *d*-axis. Before the transition, the stator current vector i_{s1} is located on the δ_1-axis. With the decreasing of $K_{\omega 1}$, the stator current vector will be gradually adjusted. When the $K_{\omega 1}$ decreases to zero, the stator current vector i_{s2} is located on the *q*-axis, which indicates that the transition process is over. Namely, φ_2 is equal to zero.

However, with the decreasing of $K_{\omega 1}$, the *q*-axis current component will be changed, which may lead to the change of the electromagnetic torque because the electromagnetic torque T_e is expressed as $(1.5 n_p \psi_{\mathrm{pm}} i_q)$. In order to control T_e unchanged during the transition, a feedforward current $i_{q\mathrm{Switch}} = K_{\omega 2} I_{\mathrm{Const}}$ needs to be added on the *q*-axis, as descried in Fig. 3. Afterward, the electromagnetic torque T_e $(K_{\omega 1}, K_{\omega 2})$ can be

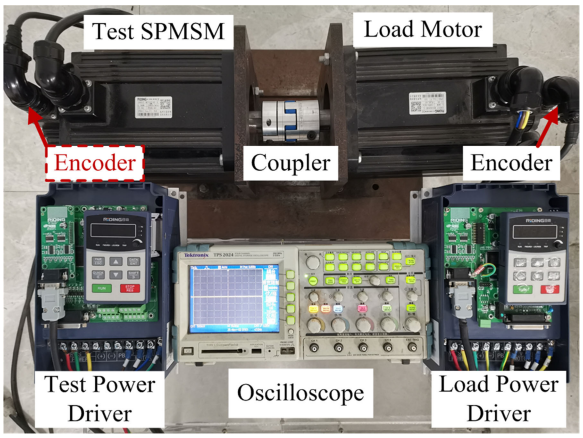

Fig. 5. Experimental setup used to test the proposed method.

deduced as (13) during the transition

$$T_e\left(K_{\omega 1}, K_{\omega 2}\right) = \frac{3}{2} n_p \psi_{\mathrm{pm}} I_{\mathrm{Const}} \left\{K_{\omega 1} \sin\left(K_{\omega 1}\varphi_2\right) + K_{\omega 2} \cos\left(K_{\omega 1}\varphi_2\right)\right\} \quad (13)$$

Because T_e should be always controlled unchanged when $K_{\omega 1}$ gradually decreases to 0 from 1, namely $T_e\left(K_{\omega 1}, K_{\omega 2}\right)$ will be always equal to the initial value $T_e\left(1, 0\right)$

$$T_e\left(K_{\omega 1}, K_{\omega 2}\right) = T_e\left(1, 0\right) \Rightarrow K_{\omega 1} \sin\left(K_{\omega 1}\varphi_2\right) + K_{\omega 2} \cos\left(K_{\omega 1}\varphi_2\right) = \sin\left(\varphi_2\left(t_0\right)\right) \quad (14)$$

where $\varphi_2(t_0)$ is the initial value of φ_2 during the transition. After simplifying (14), the relationship of $K_{\omega 1}$ and $K_{\omega 2}$ can be given as

$$K_{\omega 2} = \frac{\sin\left(\varphi_2\left(t_0\right)\right) - K_{\omega 1} \sin\left(K_{\omega 1}\varphi_2\right)}{\cos\left(K_{\omega 1}\varphi_2\right)}. \quad (15)$$

It should be noted that $\varphi_2(t_0)$ is only calculated once at the beginning of the transition. During the transition, $\varphi_2(t_0)$ is the constant. Therefore, a smooth transition from the *I–f* control to the proposed flux linkage observer-based closed-loop sensorless control can be achieved without the large torque ripple and speed fluctuation as long as the switching coefficient $K_{\omega 1}$ gradually decreases to 0 from 1 while the relationship of $K_{\omega 1}$ and $K_{\omega 2}$ satisfies (15). Furthermore, an adaptive transition can be achieved when the selection of the switching coefficient $K_{\omega 1}$ is based on the bandwidth of the current regulator.

V. Experimental Results

To verify the validity and practicability of the proposed hybrid sensorless control strategy integrating with the improved flux linkage observer and the *I–f* starting method, an experimental platform of a 5.5-kW SPMSM is utilized, as shown in Fig. 5. It consists of a test SPMSM, a load motor, and their respective power drivers. The load motor is mechanically coupled with the test SPMSM by the couplers to produce the load torque. The three-phase insulated gate bipolar translator inverter in each power driver, supplied at a dc-link voltage of 540 V, feeds the motor. An American Documentation Institute processor ADSP-CM408 is used to execute the entire control algorithm. The specification and parameters of the test SPMSM are listed in Table I. An incremental encode with resolution of 2500 line is equipped to provide the actual rotor-position, which is only used for the experimental comparison. The total block diagram of the implemented drive system is described in Fig. 3. And all the experimental results are logged via oscilloscope.

TABLE I
Motor Parameters

Parameter	SPMSM
Rated Power	5.5*kW*
Rated Speed	1500*r/min*
Rated Current	12.0*A*
Phase Resistance	0.621Ω
d-/*q*-axis Inductance	3.5*mH*
Pole Numbers	8
Rotor Magnet Flux	0.335*Wb*
Rated Voltage	380*V*
Rated Torque	35Nm
Inertia	$8.6*10^{-3}$ kg·m^2

First, in the proposed hybrid sensorless control strategy integrating with the improved flux linkage observer and the *I–f* starting method, there are four parameters needed to be designed: the gain *K* in the sliding-mode compensator, the cutoff frequency of the LPF in (3a), the cutoff frequency of the LPF in the sliding-mode compensator, and the switching coefficient $K_{\omega 1}$. In order to make the sliding-mode compensator reach to the sliding surfaces, *K* should be selected large enough, which can be approximate to $(\omega_r L_s I_{\mathrm{limit}} + \omega_r \psi_{\mathrm{pm}})$ through accessibility analysis. In which, I_{limit} is the current limit value. The LPF in (3a) is used to construct the δ–γ reference frame. Because no matter how large these angle deviations between $\theta_{r\mathrm{Est}}$ and the actual rotor-position θ_r, they can be always compensated accurately by using the sliding-mode compensator, and the cutoff frequency of this LPF can be selected properly for the fast system dynamic response. Fig. 6 shows the experimental results with different cut-off frequencies of the LPF in (3a). In the experiments, the machine runs at 750 r/min with full applied load. The cut-off frequency of the first LPF in (3a) is set as 5, 25, 50, and 75 Hz, respectively. As observed from the experimental results, the estimated rotor-position errors are little and unchangeable to the cut-off frequency, which indicates that the proposed improved flux linkage observer is robust against the LPF's cut-off frequency. Thus, in order to get the fast system dynamic response, the cut-off frequency of the first LPF in (3a) is selected as 75 Hz in this article.

The LPF in the sliding-mode compensator is adopted to get smooth $\Delta E_{\alpha\beta}$. Although this LPF has no effects on the position estimation accuracy, the cut-off frequency of the LPF affects the dynamic convergence, which will lead to the limited system bandwidth. Thus, the higher cutoff frequency of the LPF is better under the condition of assurance of the smoothness. In order to select the suitable cut-off frequency of this LPF, some experimental results have been carried out in this article, which are shown in Fig. 7. In the experiments, the machine runs at 750 r/min with full applied load. The cut-off frequency of the

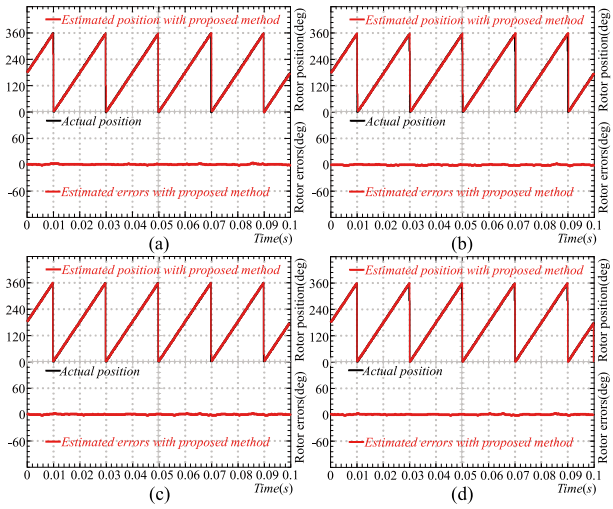

Fig. 6. Rotor-position estimation with different LPF's cut-off frequencies in (3a). (a) LPF's cut-off frequency is set as 5 Hz. (b) LPF's cut-off frequency is set as 25 Hz. (c) LPF's cut-off frequency is set as 50 Hz. (d) LPF's cut-off frequency is set as 75 Hz.

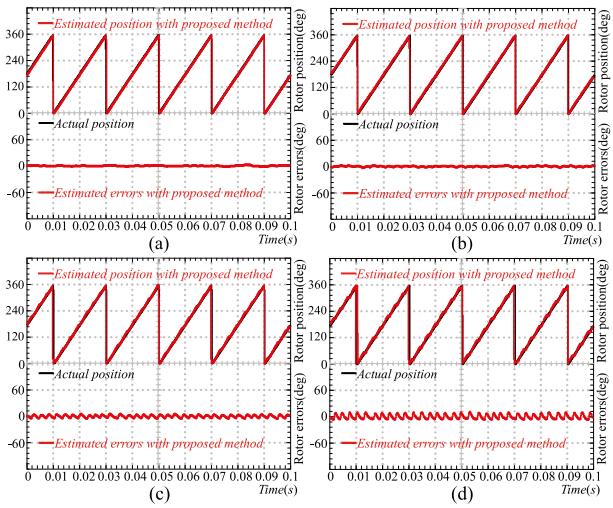

Fig. 7. Rotor-position estimation with different LPF's cut-off frequencies in the proposed sliding-mode compensator. (a) LPF's cut-off frequency is set as 50 Hz. (b) LPF's cut-off frequency is set as 100 Hz. (c) LPF's cut-off frequency is set as 200 Hz. (d) LPF's cut-off frequency is set as 300 Hz.

LPF in (7b) is set as 50, 100, 200, and 300 Hz, respectively. These curves of estimated rotor-position, actual rotor-position, and angle estimation errors are described. As observed from the experimental results, the estimated rotor-position ripples are increasing with the increase in the cut-off frequency. In order to get the rapid convergence speed and good smoothness, the cut-off frequency of this LPF in the sliding-mode compensator can be selected as 100 Hz.

As for the parameter tuning of the switching coefficient $K_{\omega 1}$, its selection is mainly based on the bandwidth of the current regulator. In order to analyze the effects of the different $K_{\omega 1}$ on the transition process, some experimental results have been carried out, which are shown in Figs. 8 and 9. It should be noted that the quicker decreasing of $K_{\omega 1}$ is better under the condition of assurance of little torque and speed ripples during

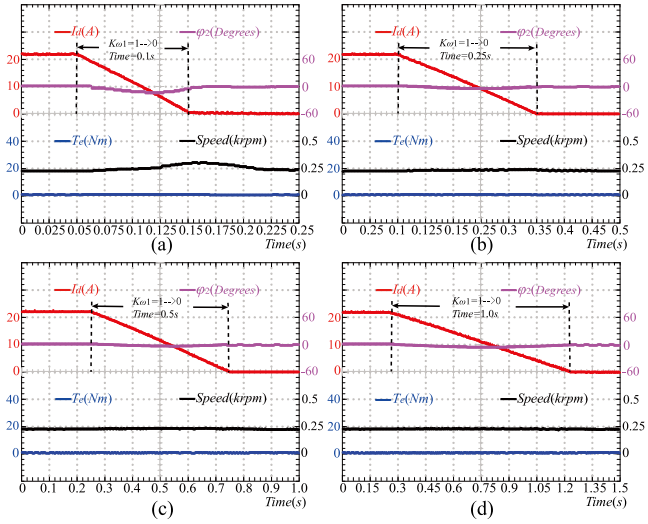

Fig. 8. Experimental results with the different decreasing time of $K_{\omega 1}$ during the transition process at light load. (a) 0.1 s. (b) 0.25 s. (c) 0.5 s. (d) 1.0 s.

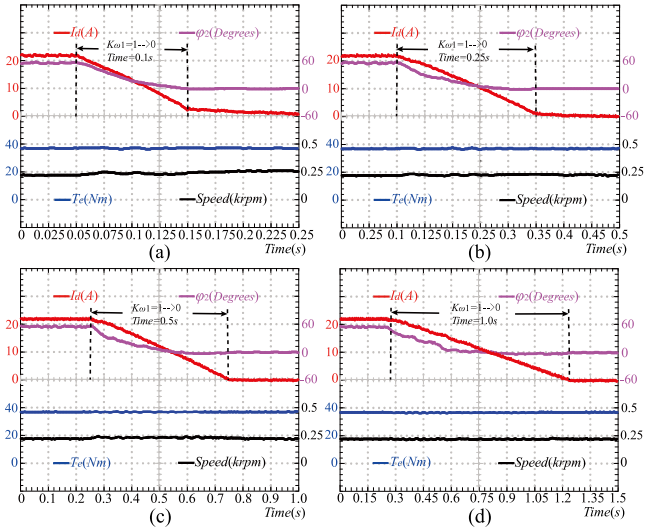

Fig. 9. Experimental results with the different decreasing time of $K_{\omega 1}$ during the transition process at full load. (a) 0.1 s. (b) 0.25 s. (c) 0.5 s. (d) 1.0 s.

the transition process. As observed from Figs. 8 and 9, when $K_{\omega 1}$ is decreasing to zero within 0.25 s, there are little torque and speed ripples at both light load and full load. Therefore, 0.25 s is selected for the decreasing of $K_{\omega 1}$ from 1 to 0 in this article. And $K_{\omega 2}$ can be determined by (15).

And then, in order to show the superiority of the proposed enhance flux linkage observer based on the sliding-mode compensator against the conventional rotor flux estimation method with the speed iterative compensation, the comparative experiments with a variable load have been done, as shown in Figs. 10 and 11. It should be noted that the calculation process of the conventional rotor flux estimation method with the speed iterative compensation can be roughly described in (3a) and (3b). In which, the desired flux linkage is computed after the filtering of the back-EMF of the machine through the LPF and the compensation of the flux generated by the stator currents. Afterward, the estimated rotor-position can be obtained by calculating the

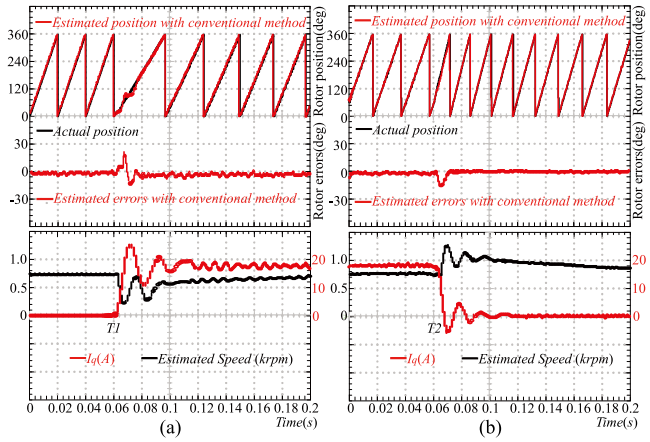

Fig. 10. Experimental results of the variable load test by using the conventional rotor flux estimation method with the speed iterative compensation. (a) Motor load is changed from no load to the rated full load. (b) Motor load is changed from the rated full load back to no load.

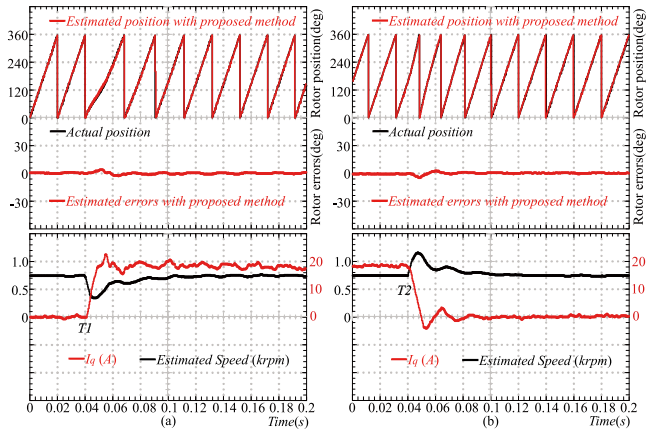

Fig. 11. Experimental results of the variable load test with the proposed improved flux linkage observer. (a) Motor load is changed from no load to the rated full load. (b) Motor load is changed from the rated full load back to no load.

phase angle of the acquired flux linkage. And then, according to the phase-frequency characteristic of the LPF, the deviation angles caused by the LPF are compensated through the speed iteration. As observed from the experimental results, in the conventional rotor flux estimation method with the speed iterative compensation, because the system dynamic response is affected by the speed iterative operation, the speed and stator current turn back to its reference value after a larger adjustment and have larger position estimation errors when the load is suddenly changed. Compared with the conventional method, because the cutoff frequency of the adopted LPF in the proposed improved flux linkage observer can be selected properly for the fast system dynamic response, the speed and stator current quickly turn back to its reference value with little position estimation errors, which indicates the proposed improved flux linkage observer can significantly improve the system dynamic performance.

To further show the effects of machine parameter variations on the proposed improved flux linkage observer, the corresponding experiments have been implemented. The machine runs at 750 r/min with full applied load. The experimental results

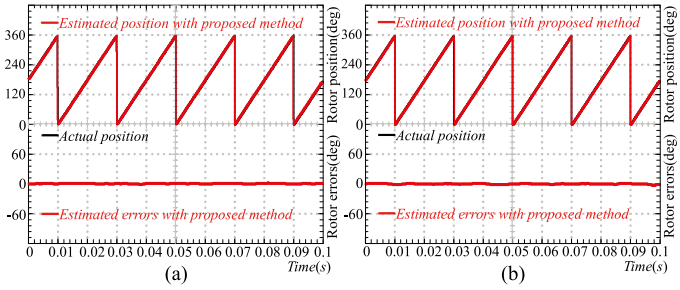

Fig. 12. Experimental results of the proposed improved flux linkage observer with the resistance variations. (a) 50% decrease. (b) 50% increase.

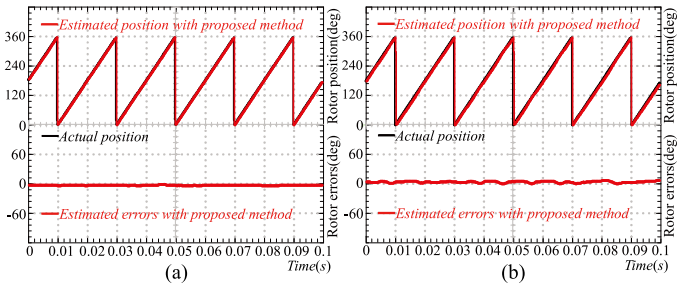

Fig. 13. Experimental results of the proposed improved flux linkage observer with the stator inductance variations. (a) 50% decrease. (b) 50% increase.

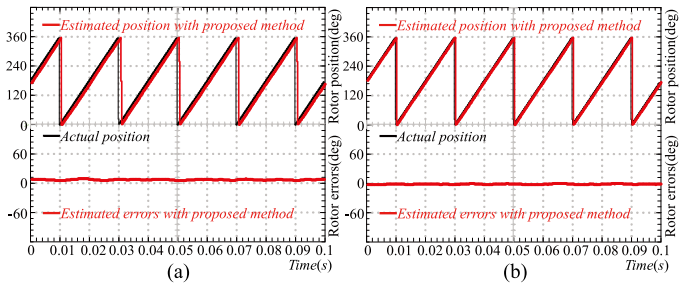

Fig. 14. Experimental results of the proposed improved flux linkage observer with the permanent-magnet flux linkage variations. (a) 50% decrease. (b) 50% increase.

are shown in Figs. 12–14. As observed from the experimental results, when the stator resistance decreases and increases 50% of the actual value, respectively, the estimated rotor-position can still converge to the actual value. And when the stator inductance is changing 50% of the actual value, there are also little angle estimation errors. The reason is that the term $L_s I_s$ is smaller relative to the permanent-magnet flux linkage $\psi_{\rm pm}$. The change of L_s cannot bring a large change in φ_{1_v} by referring to (12). However, when the permanent-magnet flux linkage is changing 50% of the actual value, the angle estimation errors are about 10 electrical degrees relative to the actual rotor-position, which is in accord with the theoretical calculation approximately by (12). However, usually the permanent-magnet flux linkage $\psi_{\rm pm}$ changes little because the machine rarely operates in the demagnetization region of the ferromagnetic material. Thus, the estimation accuracy of the rotor-position based on the proposed improved flux linkage observer can meet general application requirements even if the offline machine parameters are used. For those high-precision applications, several machine parameter identification methods should be adopted to identify L_s and $\psi_{\rm pm}$ online and accurately for higher estimation accuracy.

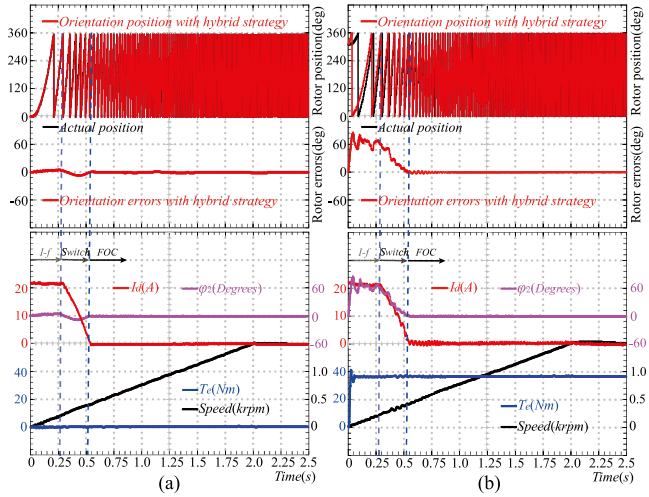

Fig. 15. Experimental results based on the proposed hybrid strategy when the machine runs from startup to the rated speed. (a) With no load. (b) With full load.

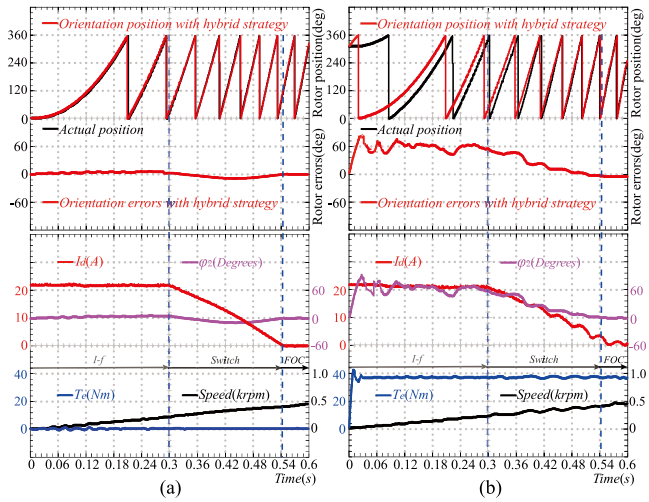

Fig. 16. Rotor-position estimation based on the proposed hybrid strategy during the accelerate procedure in the first 0.6 s. (a) With no load. (b) With full load.

In order to evaluate the full region sensorless control performance, the sensorless drive startup from the zero speed to rated speed 1500 r/min are carried out in Figs. 15 and 16. The transition starts at 15% rated speed (15 Hz), which corresponds to 0.3 s in Figs. 15 and 16. Before 0.3 s, the *I–f* starting strategy is applied. With the increase in the speed to the transition region, the presented adaptive transition algorithm is utilized. Once the transition is over, the control algorithm will be automatically switched to the speed and current double closed-loop FOC based on the proposed improved flux linkage observer. It should be noted that the initial rotor-position needs to be detected before the *I–f* starting, because these initial position errors may reduce the load capability and even lead to the system instability. For initial rotor-position detection of the PMSM, many kinds of mature solutions based on the high-frequency carrier signal injection can be referred [6]–[10]. Once the initial position information is obtained, it can be latched. These changing curves of estimated rotor-position, actual rotor-position, position orientation errors, estimated speed, *d*-axis current, and the torque are described in Fig. 15, respectively. In order to clearly observe the transition process, the acceleration process in the first 0.6 s is also descried in Fig. 16. As observed from the experimental results, although some little fluctuations can be observed during the acceleration process, the machine can operate stably from startup to the rated speed, which verifies that the proposed hybrid strategy integrating with the improved flux linkage observer and the *I–f* starting method can achieve SPMSM sensorless control in full-speed region stably and smoothly. It should be noted that the orientation errors in Fig. 15(b) are about 60 electrical angles before the transition and gradually decreases to zero after the transition, and the orientation errors in Fig. 15(a) are approximate to zero during the whole acceleration process, which is the normal transition process.

VI. Conclusion

Based on the thought of speed partition optimization and smooth transition, this article proposes a hybrid sensorless control strategy combining a robust flux linkage observer and the *I–f* starting method to improve the whole-speed-range sensorless control performance of the SPMSM. At zero and low speed, the *I–f* control method fulfills the stable startup and possesses the ability of antidisturbance to a degree through its self-stabilization between torque and power angle. At medium and high speed, an improved flux linkage observer based on the sliding-mode compensator is designed for the closed-loop sensorless operation. Taking advantage of the sliding-mode compensator, these position errors caused by the adopted filter for the elimination of dc offset and high-order harmonics can be compensated accurately without any speed iterative operation, which can effectively improve the system stability. Meanwhile, because these position errors are always compensated effectively and have no influence on the estimation accuracy of the rotor-position no matter how large they are, the cutoff frequency of the adopted LPF can be selected properly for the fast system dynamic response. In addition, the influence of machine parameter variations on the rotor-position estimation accuracy is analyzed. Furthermore, in order to achieve a smooth operation between two different control schemes, an adaptive transition algorithm is described in detail. Experimental results indicate that the proposed hybrid sensorless control strategy can show an excellent performance for both steady-state and dynamic operations in the whole speed range.

References

[1] P. D. C. Perera, F. Blaabjerg, J. K. Pedersen, and P. Thogersen, "A sensorless, stable V/f control method for permanent-magnet synchronous motor drives," *IEEE Trans. Ind. Appl.*, vol. 39, no. 3, pp. 783–791, May/Jun. 2003.

[2] Z. Tang, X. Li, S. Dusmez, and B. Akin, "A new V/f-based sensorless MTPA control for IPMSM drives," *IEEE Trans. Power Electron.*, vol. 31, no. 6, pp. 4400–4415, Jun. 2016.

[3] A. Borisavljevic, H. Polinder, and J. A. Ferreira, "Realization of the I/f control method for a high-speed permanent magnet motor," in *Proc. 19th Int. Conf. Elect. Mach.*, Rome, Italy, 2010, pp. 1–6.

[4] Z. Wang, K. Lu, and F. Blaabjerg, "A simple startup strategy based on current regulation for back-EMF-based sensorless control of PMSM," *IEEE Trans. Power Electron.*, vol. 27, no. 8, pp. 3817–3825, Aug. 2012.

[5] Y. Yu, D. Chang, X. Zheng, Z. Mi, X. Li, and C. Sun, "A stator current oriented closed-loop I-f control of sensorless SPMSM with fully unknown parameters for reverse rotation prevention," *IEEE Trans. Power Electron.*, vol. 33, no. 10, pp. 8607–8622, Oct. 2018.

[6] O. A. Mohammed, A. A. Khan, A. M. El-Tallawy, A. Nejadpak, and M. J. Roberts, "A wavelet filtering scheme for noise and vibration reduction in high-frequency signal injection-based sensorless control of PMSM at low speed," *IEEE Trans. Energy Convers.*, vol. 27, no. 2, pp. 250–260, Jun. 2012.
[7] G. Xie, K. Y. Lu, S. K. Dwivedi, J. R. Rosholm, and F. Blaabjerg, "Minimum-voltage vector injection method for sensorless control of PMSM for low-speed operations," *IEEE Trans. Power Electron.*, vol. 31, no. 2, pp. 1785–1794, Feb. 2016.
[8] S. I. Kim, J. H. Im, E. Y. Song, and R. Y. Kim, "A new rotor position estimation method of IPMSM using all-pass filter on high-frequency rotating voltage signal injection," *IEEE Trans. Ind. Electron.*, vol. 63, no. 10, pp. 6499–6509, Oct. 2016.
[9] P. Xu and Z. Q. Zhu, "Analysis of parasitic effects in carrier signal injection methods for sensorless control of PM synchronous machines," *IET Elect. Power Appl.*, vol. 12, no. 2, pp. 203–212, Feb. 2018.
[10] C. Hwang, Y. Lee, and S. Sul, "Analysis on position estimation error in position-sensorless operation of IPMSM using pulsating square wave signal injection," *IEEE Trans. Ind. Appl.*, vol. 55, no. 1, pp. 458–470, Jan./Feb. 2019.
[11] A. Zaafouri, C. B. Regaya, H. B. Azza, and A. Châari, "DSP-based adaptive backstepping using the tracking errors for high-performance sensorless speed control of induction motor drive," *ISA Trans.*, vol. 60, pp. 333–347, Jan. 2016.
[12] C. B. Regaya, F. Farhani, A. Zaafouri, and A. Chaari, "A novel adaptive control method for induction motor based on backstepping approach using dSpace DS 1104 control board," *Mech. Syst. Signal Process.*, vol. 100, pp. 466–481, Jan. 2018.
[13] G. H. B. Foo and M. F. Rahman, "Direct torque control of an IPM-synchronous motor drive at very low speed using a sliding-mode stator flux observer," *IEEE Trans. Power Electron.*, vol. 25, no. 4, pp. 933–942, Apr. 2010.
[14] O. Saadaoui, A. Khlaief, M. Abassi, A. Chaari, and M. Boussak, "Sensorless FOC of PMSM drives based on full order SMO," in *Proc. 17th Sci. Techn. Autom. Control Comput. Eng. Int. Conf.*, Sousse, Tunisia, 2016, pp. 663–668.
[15] D. Liang, J. Li, and R. Qu, "Sensorless control of permanent magnet synchronous machine based on second-order sliding-mode observer with online resistance estimation," *IEEE Trans. Ind. Appl.*, vol. 53, no. 4, pp. 3672–3682, Jul./Aug. 2017.
[16] O. C. Kivanc and S. B. Ozturk, "Sensorless PMSM drive based on stator feedforward voltage estimation improved with MRAS multiparameter estimation," *IEEE/ASME Trans. Mechatronics*, vol. 23, no. 3, pp. 1326–1337, Jun. 2018.
[17] E. Zerdali, "Adaptive extended kalman filter for speed-sensorless control of induction motors," *IEEE Trans. Energy Convers.*, vol. 34, no. 2, pp. 789–800, Jun. 2019.
[18] S. Yang and Y. Hsu, "Full speed region sensorless drive of permanent-magnet machine combining saliency-based and back-EMF-based drive," *IEEE Trans. Ind. Electron.*, vol. 64, no. 2, pp. 1092–1101, Feb. 2017.
[19] Y. Sun, M. Preindl, S. Sirouspour, and A. Emadi, "Unified wide-speed sensorless scheme using nonlinear optimization for IPMSM drives," *IEEE Trans. Power Electron.*, vol. 32, no. 8, pp. 6308–6322, Aug. 2017.
[20] A. Yousefi-Talouki, P. Pescetto, G. Pellegrino, and I. Boldea, "Combined active flux and high-frequency injection methods for sensorless direct-flux vector control of synchronous reluctance machines," *IEEE Trans. Power Electron.*, vol. 33, no. 3, pp. 2447–2457, Mar. 2018.
[21] K. Cho and J. Seok, "Pure-integration-based flux acquisition with drift and residual error compensation at a low stator frequency," *IEEE Trans. Ind. Appl.*, vol. 45, no. 4, pp. 1276–1285, Jul./Aug. 2009.
[22] Y. Wang and Z. Deng, "An integration algorithm for stator flux estimation of a direct-torque-controlled electrical excitation flux-switching generator," *IEEE Trans. Energy Convers.*, vol. 27, no. 2, pp. 411–420, Jun. 2012.
[23] A. Khlaief, O. Saadaoui, M. Boussak, and A. Chaari, "Implementation of stator resistance adaptation for sensorless speed control of IPMSM drive based on nonlinear position observer," in *Proc. 22nd Elect. Mach. Int. Conf.*, Lausanne, Switzerland, 2016, pp. 1071–1077.
[24] Z. Xin, R. Zhao, F. Blaabjerg, L. Zhang, and P. C. Loh, "An improved flux observer for field-oriented control of induction motors based on dual second-order generalized integrator frequency-locked loop," *IEEE J. Emerg. Sel. Topics Power Electron.*, vol. 5, no. 1, pp. 513–525, Mar. 2017.
[25] D. Wang, K. Lu, and P. O. Rasmussen, "Improved closed-loop flux observer based sensorless control against system oscillation for synchronous reluctance machine drives," *IEEE Trans. Power Electron.*, vol. 34, no. 5, pp. 4593–4602, May 2019.
[26] J. Choi, K. Nam, A. A. Bobtsov, and R. Ortega, "Sensorless control of IPMSM based on regression model," *IEEE Trans. Power Electron.*, vol. 34, no. 9, pp. 9191–9201, Sep. 2019.
[27] G. Jo and J. Choi, "Gopinath model-based voltage model flux observer design for field-oriented control of induction motor," *IEEE Trans. Power Electron.*, vol. 34, no. 5, pp. 4581–4592, May 2019.
[28] M. A. Hamida, J. De Leon, A. Glumineau, and R. Boisliveau, "An adaptive interconnected observer for sensorless control of PM synchronous motors with online parameter identification," *IEEE Trans. Ind. Electron.*, vol. 60, no. 2, pp. 739–748, Feb. 2013.
[29] T. Boileau, N. Leboeuf, B. Nahid-Mobarakeh, and F. Meibody-Tabar, "Online identification of PMSM parameters: Parameter identifiability and estimator comparative study," *IEEE Trans. Ind. Appl.*, vol. 47, no. 4, pp. 1944–1957, Jul./Aug. 2011.
[30] Z. Liu, X. Li, L. Wu, S. Zhou, and K. Liu, "GPU-accelerated parallel coevolutionary algorithm for parameters identification and temperature monitoring in permanent magnet synchronous machines," *IEEE Trans. Ind. Inform.*, vol. 11, no. 5, pp. 1220–1230, Oct. 2015.

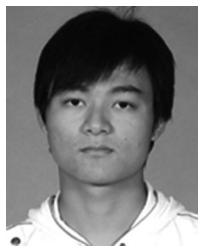

Qipeng Tang was born in Jiangxi, China, in 1991. He received the B.S. and Ph.D. degree from the School of Automation, Huazhong University of Science and Technology, Wuhan, China, in 2013 and 2018, Respectively.

From 2018, he joined the College of Electrical Engineering, Zhejiang University as a Postdoctoral Researcher.

His research interests include power electronics, high-performance ac motor drives, and sensorless control for electrical drives.

Duxin Chen (Member, IEEE) received the B.S. degree in automatic control and the Ph.D. degree in control science and engineering from the Huazhong University of Science and Technology, Wuhan, China, in 2013 and 2018, respectively.

He is currently an Assistant Professor with the School of Automation, Southeast University, Nanjing, China. His research interests include nonlinear control, complex networks, networked control systems, and its applications.

Xiangning He (Fellow, IEEE) received the B.Sc. and M.Sc. degrees from the Nanjing University of Aeronautical and Astronautical, Nanjing, China, in 1982 and 1985, respectively, and the Ph.D. degree from Zhejiang University, Hangzhou, China, in 1989.

From 1985 to 1986, he was an Assistant Engineer with the 608 Institute of Aeronautical Industrial General Company, Zhuzhou, China. From 1989 to 1991, he was a Lecturer with Zhejiang University. In 1991, he obtained a fellowship from the Royal Society of U.K. and conducted research in the Department of Computing and Electrical Engineering, Heriot-Watt University, Edinburgh, U.K., as a Postdoctoral Research Fellow for two years. In 1994, he joined Zhejiang University as an Associate Professor, where he has been a Full Professor with the College of Electrical Engineering, the Director of the Power Electronics Research Institute, and the Head of the Department of Applied Electronics since 1996, and is currently the Vice Dean of the College of Electrical Engineering. He has authored or coauthored more than 280 papers and one book *Theory and Applications of Multi-Level Converters*, China Machine Press, Aug. 2006. He holds 22 patents. His research interests include power electronics and their industrial applications.

Dr. He was the recipient of the 1989 Excellent Ph.D. Graduate Award, the 1995 Elite Prize Excellence Award, the 1996 Outstanding Young Staff Member Award, and 2006 Excellent Staff Award from Zhejiang University for his teaching and research contributions. He received seven Scientific and Technological Achievements Awards from Zhejiang Provincial Government and the State Educational Ministry of China in 1998, 2002, 2009, and 2011 and six excellent paper awards. He has been appointed as IEEE Distinguished Lecturer by the IEEE Power Electronics Society in 2011. He is also a Fellow of the Institution of Engineering and Technology (formerly IEE), U.K.